Few-Electron Ultrastrong Light-Matter Coupling in a Quantum *LC* Circuit

Yanko Todorov and Carlo Sirtori

Université Paris Diderot, Sorbonne Paris Cité, Laboratoire Matériaux et Phénomènes Quantiques, CNRS-UMR 7162, 75013 Paris, France

(Received 19 March 2014; revised manuscript received 23 October 2014; published 18 November 2014)

The phenomenon of ultrastrong light-matter interaction of a two-dimensional electron gas within a lumped element electronic circuit resonator is explored. The gas is coupled through the oscillating electric field of the capacitor, and in the limit of very small capacitor volumes, the total number of electrons of the system can be reduced to only a few. One of the peculiar features of our quantum mechanical system is that its Hamiltonian evolves from the fermionic Rabi model to the bosonic Hopfield model for light-matter coupling as the number of electrons is increased. We show that the Dicke states, introduced to describe the atomic super-radiance, are the natural base to describe the crossover between the two models. Furthermore, we illustrate how the ultrastrong coupling regime in the system and the associated antiresonant terms of the quantum Hamiltonian have a fundamentally different impact in the fermionic and bosonic cases. In the intermediate regime, our system behaves like a multilevel quantum bit with nonharmonic energy spacing, owing to the particle-particle interactions. Such a system can be inserted into a technological semiconductor platform, thus opening interesting perspectives for electronic devices where the readout of quantum electrodynamical properties is obtained via the measure of a DC current.

DOI: 10.1103/PhysRevX.4.041031

Subject Areas: Condensed Matter Physics, Nanophysics, Quantum Physics

I. INTRODUCTION

The strong light-matter coupling regime is a well-known concept in quantum electrodynamics [1]. This occurs when a material excitation reversibly exchanges its energy with an optical mode of a microcavity, and it has so far been realized in numerous physical systems, such as atoms in microwave cavities [2,3], excitons in semiconductor quantum wells (QW) [4] or quantum boxes [5,6], superconducting circuits [7–9], and optomecanical resonators [10]. Recently, there have been several theoretical studies of the ultrastrong light-matter interaction regime [11–13] where the coupling constant, also called Rabi frequency, Ω_R, becomes comparable with the energy of the material excitation. This regime has been realized experimentally with intersubband transitions coupled with plasmon waveguides in the midinfrared (MIR) [14] and metallic microcavities in the terahertz (THz) frequency range [15–17], magnetoplasmons of two-dimensional electron gas [18], superconducting qubits [19], and molecular transitions [20].

However, all these experimental and theoretical studies refer to two completely different models depicting the strong light-matter coupling regime. The first corresponds to the Rabi model [21,22], which describes the interaction of a two-level system with a quantum harmonic oscillator. In the context of quantum optics, the harmonic oscillator corresponds to a single mode of the electromagnetic field, and this model, often combined with a rotating-wave approximation, is also well known as the Jaynes-Cummings model [23]. The second model is the polariton Hopfield model [24], where the electromagnetic field interacts with a collective material polarization. In the latter, both material excitation and the electromagnetic field are described as boson fields with harmonic excitation spectra. The Rabi model is pertinent to describe experiments in atomic physics [2,3], superconducting qubits [7–9], or dielectric microcavities coupled with quantum boxes [5,6]. The Hopfield model describes well the propagation of light in solids [25], as well as recent experiments with microcavities interacting with confined plasmons in the infrared part of the spectrum [15–17]. In the present work, we describe a quantum-mechanical system that can be continuously tuned between the Rabi model and the Hopfield polariton model, by changing the number of electronic transitions resonantly coupled with the electromagnetic field. We show that the Dicke states, introduced to describe the atomic super-radiance [26], play a crucial role to account for the fermionic-bosonic crossover. Furthermore, by exploring the properties of the ultrastrong coupling regime in our system, we illustrate clearly the fundamental difference between the fermionic Rabi model and the bosonic Hopfield description.

Our system is set to operate in the THz part of the spectrum, where, quite remarkably, another fundamental crossover takes place: the transition between optics and electronics. Indeed, in the THz range, metals can be commonly used to confine light [27], and the realization of electromagnetic resonators can be inspired either by photonic or electronic concepts. The use of metals permits us to confine the light in photonic resonators with a very small effective volume V, much smaller than what can be achieved using dielectrics. However, even in this case, at least one of the resonator dimensions must be commensurable with the resonant wavelength λ, which, in principle, sets the ultimate limit for the light confinement based on a photonic resonator. No such limitation exists for an electronic circuit resonator built of lump elements with physical sizes that are much smaller than the resonant wavelength [28]. As the light-matter coupling constant Ω_R scales like $1/\sqrt{V}$ [1,29], it is very interesting to explore and understand the limit towards an arbitrarily small volume. This limit is the bases of our quantum-mechanical system consisting of a collection of electronic intersubband dipoles coupled to the oscillating electric field in an "*LC*" (inductance-capacitor) resonant circuit. We will show that, indeed, the interaction strength Ω_R becomes very large when the capacitor volume is reduced, leading to the regime of ultrastrong light-matter coupling with just a few electrons. In principle, the only limitation to the coupling strength in this case is the size of the quantum structure that confines the electrons. We show that in such a system, the nature of the coupling is profoundly modified by the number of dipoles interacting with light. If the system is composed of a very large number of dipoles, the electronic ensemble behaves like a confined plasmon with bosonic character. In the opposite limit of a few dipoles, the system can no longer be described by bosons but rather as a collection of two-level systems eventually coupled through interparticle interactions. The quantum description of the system that we present therefore allows one to bridge condensed-matter many-body collective excitations with quantum optics and atomic physics.

Our paper is organized as follows. In Sec. II, we discuss a representation of the fundamental electromagnetic Hamiltonian that captures the transition between optics and electronics. In Sec. III, we apply our Hamiltonian to describe the interaction between an *LC* circuit and a two-dimensional electron gas, coupled through the circuit capacitor, and we explore the system while varying the number of electrons in the gas. We demonstrate the crossover between the fermionic and bosonic nature of the light-coupled excitations of the gas, and we provide the corresponding features while the system operates in the ultrastrong circuit-matter coupling regime. Much of the technical information is gathered in the Appendixes.

II. TRANSITION BETWEEN OPTICS AND ELECTRONICS: HAMILTONIAN DESCRIPTION

We will start our analysis by recalling the classical description of an electromagnetic resonator, which is based on the periodic energy exchange between the magnetic and electric fields. What distinguishes the photonic from the circuit resonator is how this exchange takes place. The physics of the phenomenon is contained in the fourth Maxwell equation [28,30]:

$$\nabla \times \mathbf{H} = J + \frac{\partial \mathbf{D}}{\partial t}. \tag{1}$$

The crossover between electronics and photonics appears in the relative weight of the two source terms: the real current J and the displacement current $\partial\mathbf{D}/\partial t$. In a purely dielectric resonator [31], the current source J is absent since there are no free charges in the material. Then, according to Eq. (1), the spatial variations of the magnetic field are coupled to the temporal variations of the electric field. This entanglement between time and space, which is also present in the first Maxwell equation, $\nabla \times \mathbf{E} = -\partial\mathbf{H}/\partial t$, is the essence of propagation, and the resonator exists because it can fit a propagating wave in at least one direction. In this direction, the size of the resonator is therefore ultimately limited by $\lambda/2n$, where n is the refractive index of the material filling the resonator. On the contrary, in an oscillating circuit, the propagation effects are too small, and the displacement current can be neglected in Eq. (1). In this quasistatic limit, the oscillations arise from the physical current J that tends to compensate the electric charges on the capacitor plate. This current would induce a magnetic field in the inductance, which in turn will tend to decay, yielding a current.

From the point of view of Lagrangian quantum electrodynamics, the fundamental difference between photonic and electronic resonators corresponds to two different choices for pairs of conjugated dynamical variables. These two limits can be recovered in the dipolar Power-Zineau-Wooley (PZW) representation, where the electromagnetic Hamiltonian is expressed in terms of fields rather than vector and scalar potentials [32,33]. Furthermore, when a long-wavelength approximation is assumed, the dipole gauge permits us to obtain the relevant terms of electromagnetic interactions, as dipole-dipole and dipole-field interactions [34,35]. Let us consider an *LC* circuit as described in Fig. 1(a). In the PZW framework, the Hamiltonian of the electromagnetic field of the resonator in all space can be written as

$$\mathcal{H}_{\text{field}} = \int \frac{\mathbf{D}_\perp^2}{2\varepsilon_0} d^3\mathbf{r} + \int \frac{\mu_0 \mathbf{H}^2}{2} d^3\mathbf{r} + \int \frac{\mathbf{P}_C^2}{2\varepsilon_0 \varepsilon} d^3\mathbf{r}. \tag{2}$$

The first two terms on the right-hand side describe the energy stored in the electric and magnetic fields; however,

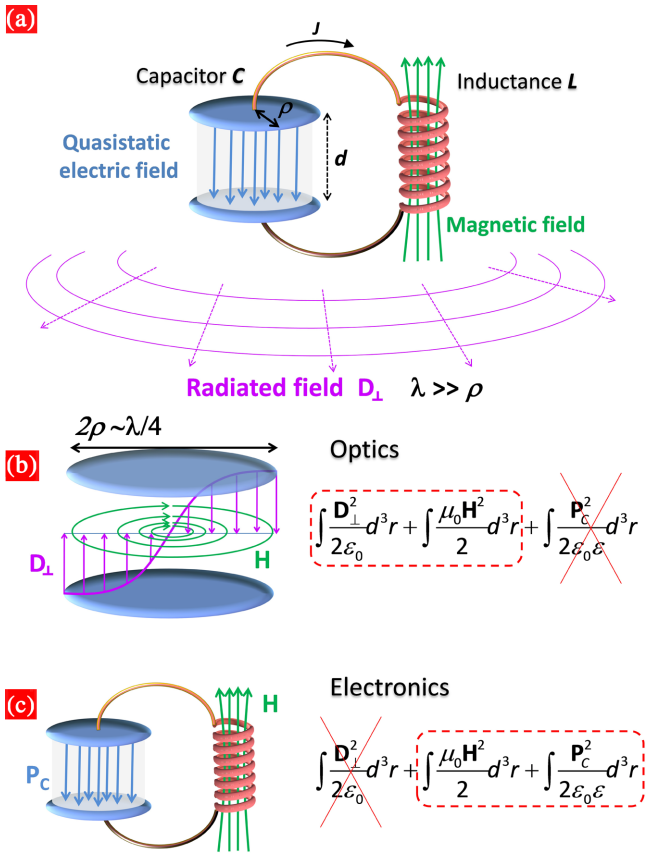

FIG. 1. (a) General illustration of an LC circuit, indicating the quasistatic electric field inside the capacitor and the radiated field far away from the system. We have considered a circular plate capacitor of radius ρ. (b,c) Relevant terms of the electrodynamic Hamiltonian that describes the system, either as a high-frequency photonic resonator (b) or a low-frequency circuit resonator (c).

while $\mathbf{H}$ describes the total magnetic field, $\mathbf{D}_\perp$ now describes only the transverse displacement field [33]. In Eq. (2), ε_0 and μ_0 are, respectively, the electric and magnetic constants. In the low-frequency limit, $\mathbf{D}_\perp$ corresponds to the field that is radiated away from the circuit [Fig. 1(a)]. The third term is the energy stored in the capacitor, owing to the presence of charges on the plates. In the dipole gauge, this energy is expressed through a polarization field $\mathbf{P}_C$ that can be obtained from the Gauss theorem (ε is the dielectric constant of the capacitor core). This is actually another way to express the longitudinal quasistatic electric field with force lines that start and terminate at the electric charges.

Two limiting cases can be extracted from $\mathcal{H}_{\text{field}}$. When at least one of the dimensions of the system is commensurable with the wavelength in the material λ/n, propagation effects are dominant. The capacitor behaves as a resonant cavity, and the electromagnetic fields $\mathbf{D}_\perp$ and $\mathbf{H}$ are essentially localized within it [Fig. 1(b)] [28]. Furthermore, $\mathbf{P}_C$ can be neglected as it is confined within the skin depth of the metal plates. Note that $\mathbf{P}_C$ is completely absent for purely dielectric microcavities or in ideal cases such as cavities made of perfect conductors. In all these cases, the conjugated dynamical variables of the system are $\mathbf{D}_\perp$ and $\mathbf{H}$. One then retains only the first two terms in Eq. (2), and the electromagnetic field is quantized by defining creation and annihilation operators a and $a^\dagger$ describing propagating photons as the elementary excitations of the field [36]. Electric and magnetic fields are thus confined in the volume V, which is necessarily *identical* for both fields.

The situation changes drastically if we consider the low-frequency limit of the LC system, where the circuit size l_{circuit} becomes much smaller than the resonant wavelength. In this case, the system can be considered as an electrically small antenna for which the radiation losses decrease strongly with the ratio $l_{\text{circuit}}/\lambda$ [Fig. 1(b)] [37]. In this limit of a "lumped" circuit, $\mathbf{D}_\perp$, which describes the field radiated away from the oscillating charges and the current loop can be neglected in Eq. (2). The second and third terms can be expressed through the magnetic flux ϕ in the inductance and the charge q on the capacitor plates, which are now the conjugated dynamical variables of the system. Equation (2) becomes [Fig. 1(c)]

$$\mathcal{H}_{\text{field}} \approx \int \frac{\mu_0 \mathbf{H}^2}{2} d^3\mathbf{r} + \int \frac{\mathbf{P}_C^2}{2\varepsilon_0 \varepsilon} d^3\mathbf{r} = \frac{\phi^2}{2L} + \frac{q^2}{2C}. \quad (3)$$

The system is now quantized as a quantum harmonic oscillator with a frequency $\omega_c = 1/\sqrt{LC}$ [36,38], and we can define raising and lowering operators $a^\dagger$ and a that create or destroy an electrical oscillation with an energy $\hbar\omega_c$ [38]. The variables q and ϕ become quantum operators expressed as $q = i\sqrt{\hbar/2Z}(a^\dagger - a)$ and $\phi = \sqrt{\hbar Z/2}(a^\dagger + a)$, with $Z = \sqrt{L/C}$ the circuit impedance. The Hamiltonian becomes $\mathcal{H}_{\text{field}} = \hbar\omega_c(a^\dagger a + 1/2)$, which is formally identical to that of propagating photons. However, in this case, the quanta of the field do not represent propagating photons with spatially entangled electric and magnetic fields, but rather "circuit photons." These "photons" correspond to an electric and a magnetic field that evolve in two distinct regions of the space but are still correlated in time. The polarization field operator $\mathbf{P}_C$ that describes the quasistatic electric field between the capacitor plates is expressed through the operators $a^\dagger$ and a:

$$\mathbf{P}_C = \mathbf{n}\varepsilon\varepsilon_0 \frac{q}{Cd} = \mathbf{n} i \sqrt{\frac{\varepsilon\varepsilon_0\hbar\omega_c}{2V}}(a^\dagger - a). \quad (4)$$

Here, d is the distance between the capacitor plates [Fig. 1(a)], and $\mathbf{n}$ is the normal to the plates. We have used the formula $C = \varepsilon\varepsilon_0 S/d$, where S is the surface of the capacitor plates ($S = \pi\rho^2$ for the system in Fig. 1). It is assumed that the polarization is homogeneous inside the capacitor volume $V = S \times d$. Since the volume of the capacitor that contains the electric field is totally

independent from the volume of the inductance, where the magnetic field develops, these two volumes can now be varied freely while maintaining the total energy of the system that is equal to a quantum $\hbar\omega_c$, a situation that is in sharp contrast with the case of propagating photons.

III. COUPLING WITH MATTER AND DICKE STATES

Our aim is now to explore the ultrastrong coupling of the circuit resonator with a material excitation. Our analysis will be performed on a model system similar to those previously used to demonstrate strong light-matter coupling in the THz and MIR ranges, where a microcavity mode is coupled with the electronic excitation of a highly doped quantum well [15–17]. We therefore focus on the case described in Fig. 2(a), where the QW is inserted inside the capacitor. There are at least two confined subbands in the well, and the fundamental subband hosts a two-dimensional electron gas (2DEG) with a total number of N_e electrons. The kinetic energy of the electron gas is provided by the Hamiltonian $\mathcal{H}_e = \sum_{\mathbf{k}} (\hbar\omega_{1\mathbf{k}} c^\dagger_{1\mathbf{k}} c_{1\mathbf{k}} + \hbar\omega_{2\mathbf{k}} c^\dagger_{2\mathbf{k}} c_{2\mathbf{k}})$, where $c^\dagger_{i\mathbf{k}}/c_{i\mathbf{k}}$ are the fermionic creation/annihilation operators in the subband state $i = 1, 2$ with an in-plane momentum $\mathbf{k}$. The energy of each state is $\hbar\omega_{i\mathbf{k}} = \hbar\omega_i + \hbar^2\mathbf{k}^2/2m^*$, with m^* the effective electron mass. The two subbands can be coupled by the oscillating electric field of the circuit provided by Eq. (4). In order to obtain this coupling, we make use of the dynamic intersubband polarization associated with the quantum transition between the subbands [35]:

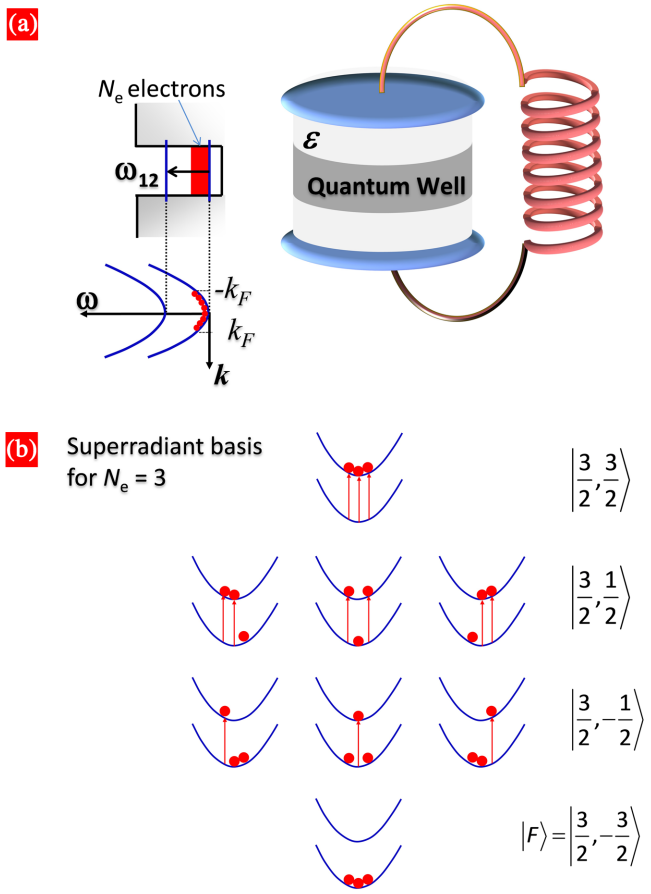

FIG. 2. (a) Illustration of a quantum well inserted into the capacitive part of an *LC* resonator and interacting with the quasistatic electric field of the capacitor. The QW is intentionally doped such that there is a two-dimensional electron gas on the first subband of the well. The energy difference between the first and the second subband, $\hbar\omega_{21}$, is matched with the resonance of the *LC* circuit, $\hbar\omega_c$. (b) Mapping of the Dicke states $|J, M\rangle$ into the possible excited states of the QW in the case of $N_e = 3$ electrons in the well.

$$\mathbf{P}_{\text{isb}} = \frac{e\hbar}{2m^* S}\sum_{\mathbf{k}} (c^\dagger_{2\mathbf{k}} c_{1\mathbf{k}} + c^\dagger_{1\mathbf{k}} c_{2\mathbf{k}}) \frac{\xi_{21}(z)}{\omega_{21}}\mathbf{n}. \quad (5)$$

Here, $\xi_{21}(z) = \varphi_2(z)\partial_z\varphi_1(z) - \varphi_1(z)\partial_z\varphi_2(z)$ is the matrix element of the microscopic current between the quantized states with wave functions $\varphi_{1,2}(z)$, and $\omega_{21} = \omega_{2\mathbf{k}} - \omega_{1\mathbf{k}}$ is the intersubband transition frequency. The homogeneous electric field of the capacitor induces strictly vertical transitions between the subbands, as shown in Eq. (5).

In the systems considered so far [15–17], strong light-matter interaction arises from the coupling between the electronic polarization $\mathbf{P}_{\text{isb}}$ [Eq. (5)] and the field $\mathbf{D}_\perp$ of a microcavity or a waveguide. As in the circuit, the propagating field can be neglected; light-matter coupling is now driven by a different mechanism that can still be derived from the Hamiltonian (3). Indeed, for the case depicted in Fig. 2(a), the polarization of the electron gas $\mathbf{P}_{\text{isb}}$ contributes to the total polarization field inside the capacitor. Therefore, in Eq. (3), we must replace $\mathbf{P}_C$ with the total polarization $\mathbf{P}_C + \mathbf{P}_{\text{isb}}$. The coupling between the electron gas and the oscillating field of the capacitor is now derived from the cross polarization term $\mathbf{P}_C \cdot \mathbf{P}_{\text{isb}}$ that appears while expanding the term $(\mathbf{P}_C + \mathbf{P}_{\text{isb}})^2$. By adding the kinetic energy of the electrons $\mathcal{H}_e$ to Eq. (3), we obtain the complete Hamiltonian describing our system:

$$\begin{aligned}\mathcal{H} &= \mathcal{H}_e + \int \frac{\mu_0 \mathbf{H}^2}{2} d^3\mathbf{r} + \int \frac{(\mathbf{P}_C + \mathbf{P}_{\text{isb}})^2}{2\varepsilon_0\varepsilon} d^3\mathbf{r} \\ &= \mathcal{H}_e + \hbar\omega_c(a^\dagger a + 1/2) + \mathcal{H}_{\text{int}} + \mathcal{H}_{\text{P2}}. \end{aligned} \quad (6)$$

Here, we introduced the interaction Hamiltonian $\mathcal{H}_{\text{int}}$ and the "depolarization" Hamiltonian $\mathcal{H}_{\text{P2}}$:

$$\begin{aligned}\mathcal{H}_{\text{int}} &= \int \frac{\mathbf{P}_C \mathbf{P}_{\text{isb}}}{\varepsilon\varepsilon_0} d^3\mathbf{r} \\ &= i\hbar\Omega_R \sqrt{\frac{\omega_c}{\omega_{21}}} \sum_{\mathbf{k}} (c^\dagger_{2\mathbf{k}} c_{1\mathbf{k}} + c^\dagger_{1\mathbf{k}} c_{2\mathbf{k}})(a^\dagger - a), \end{aligned} \quad (7)$$

$$\mathcal{H}_{\mathrm{P2}} = \int \frac{\mathbf{P}_{\mathrm{isb}}^2}{2\varepsilon\varepsilon_0} d^3\mathbf{r} = \frac{\omega_{P1}^2}{4\omega_{21}} \sum_{\mathbf{k},\mathbf{k}'} (c_{2\mathbf{k}}^\dagger c_{1\mathbf{k}} + c_{1\mathbf{k}}^\dagger c_{2\mathbf{k}})(c_{2\mathbf{k}'}^\dagger c_{1\mathbf{k}'} + c_{1\mathbf{k}'}^\dagger c_{2\mathbf{k}'}). \tag{8}$$

All the sums over the wave vectors $\mathbf{k}$ are performed on the fundamental state of the gas, which is a Fermi circle with a radius k_F. For simplicity, we neglect here the exchange-correlation interactions, and we suppose that the ground state is $|F\rangle = \prod_{|\mathbf{k}|\leq k_F} c_{1\mathbf{k}}^\dagger |0\rangle$. In these expressions, we have introduced two important quantities, Ω_R and ω_{P1}, that quantify the interaction. The first one is the circuit-matter coupling constant Ω_R:

$$\Omega_R = \sqrt{\frac{e^2 f_{21}}{4m^*\varepsilon\varepsilon_0 Sd}}, \tag{9}$$

with $f_{21} = (\hbar/2m^*\omega_{21})(\int \xi_{21}(z)dz)^2$ the oscillator strength of the intersubband transition. The second one is the coefficient ω_{P1} introduced in Eq. (8), and it is defined as

$$\omega_{P1}^2 = \frac{e^2}{\varepsilon\varepsilon_0 m^* S L_{21}}, \tag{10}$$

with $L_{21}^{-1} = (\hbar/2m^*\omega_{21}) \int \xi_{21}^2(z)dz$ the effective length of the QW renormalized by Coulomb effects [35]. Note that both of these coefficients refer to a single electron. We call ω_{P1} "one electron plasma frequency," for reasons that will be apparent in a moment.

In previous works dealing with the interaction between microcavity modes and electron gases [15–17], the coupling constants were enhanced by using very high electronic densities. In this limit, the problem contained in Eqs. (6)–(10) is not only a problem of quantum optics, referring to the term $\mathcal{H}_{\mathrm{int}}$, but also an intrinsic many-body problem due to the interaction among the electrons, described by the term $\mathcal{H}_{\mathrm{P2}}$. In our case, the many-body problem can be solved exactly, as the electric field of the capacitor is considered to be homogeneous; therefore, no momentum is exchanged between the many-body states and the circuit photons. Furthermore, in the parabolic-band approximation, the transition frequency $\omega_{21} = \omega_{2\mathbf{k}} - \omega_{1\mathbf{k}}$ is independent from the electronic wave vector $\mathbf{k}$, and all the electrons interact with the electric field at the same energy. The system that we are investigating is therefore very similar to the atomic ensemble first studied by Dicke [26,39] to explain the superradiant emission. In the case of the atomic super-radiance, different atoms are labeled according to their positions in space, and the atomic cloud is localized in a region much smaller than the wavelength. In our case [Fig. 2(a)], all electrons have the same envelope wave functions $\varphi_{1,2}(z)$ along the growth direction z. However, in the plane, they are delocalized waves $\exp(i\mathbf{kr})/\sqrt{S}$ with different momenta $\mathbf{k}$ due to the Pauli exclusion principle. The electronic states are thus labeled according to their momentum states $\mathbf{k}$ instead of their positions, with parabolic dispersion as shown in Fig. 2(a). In analogy with atomic clouds, we can then define raising and lowering superradiant operators that act in the momentum space rather than the position space:

$$D^+ = \sum_{\mathbf{k}} c_{2\mathbf{k}}^\dagger c_{1\mathbf{k}}, \qquad D^- = \sum_{\mathbf{k}} c_{1\mathbf{k}}^\dagger c_{2\mathbf{k}}. \tag{11}$$

The Hamiltonians $\mathcal{H}_{\mathrm{int}}$ and $\mathcal{H}_{\mathrm{P2}}$ can now be conveniently expressed as $\mathcal{H}_{\mathrm{int}} = i\hbar\Omega_R\sqrt{\omega_c/\omega_{21}}(D^+ + D^-)(a^\dagger - a)$ and $\mathcal{H}_{\mathrm{P2}} = \hbar\omega_{P1}^2/4\omega_{21}(D^+ + D^-)^2$. If we ignore the $\mathcal{H}_{\mathrm{P2}}$ part, Eq. (6) corresponds exactly to the Dicke Hamiltonian. In this case, the collective states interacting with light can be mapped into the angular momentum states $|J, M\rangle$ of N_e spins $s = 1/2$ with total angular momentum $J = N_e/2$ and spin projections $M = -J \ldots J$. The fundamental state of the electron gas, where all electrons occupy the first subband, is then $|F\rangle = |J, -J\rangle$. The excited states of the system are described by $|J, M\rangle$ with $M > -J$, and they correspond to coherent superpositions of all states with $J + M$ electrons excited on the second subband [Fig. 2(b)]. These states are obtained by applying $J + M$ times the operator D^+ on the ground state $|F\rangle$ (see Appendix A). By using the commutation relations $[\mathcal{H}_{\mathrm{e}}, D^\pm] = \pm\hbar\omega_{21}D^\pm$, it is easily shown that $|J, M\rangle$ is an eigenvector of the electronic Hamiltonian $\mathcal{H}_{\mathrm{e}}$ with an eigenvalue $E_G + (J + M)\hbar\omega_{21}$, where E_G is the ground-state energy. In Fig. 2(b), we illustrate the mapping between the excited states of the electron gas and the angular momentum states $|J, M\rangle$ for the case of an $N_e = 3$ electron system.

Let us then consider a situation where the system is probed by a weak excitation, and only the transition between the fundamental and the first excited state $|J, -J + 1\rangle$ is relevant. Then, it is well known from the theory of super-radiance [39] that the N_e electrons interact collectively with light with an effective coupling constant $\Omega_{R\mathrm{eff}} = \Omega_R\sqrt{N_e}$. This coupling constant $\Omega_{R\mathrm{eff}}$ is identical to that of a photonic resonator operating in the fundamental transverse-magnetic TM_0 mode of a double-metal waveguide of a thickness d and volume $V = Sd$ [15]. The major difference is that now the surface of the capacitor S is no longer tied to propagation effects and could be made arbitrary small. One can therefore envision the case where S is strongly reduced while keeping the areal density N_e/S very high and constant. In this limit, a very high coupling energy $\hbar\Omega_{R\mathrm{eff}}$ can be obtained while the number of electrons in the system is highly reduced.

The reduction of the surface S also implies a reduction of the capacitance C, which in turn changes the resonant frequency $\omega_c = 1/\sqrt{LC}$ of the LC circuit. In order to keep

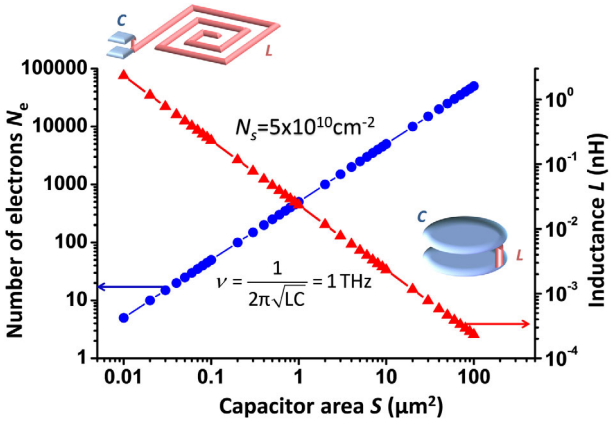

FIG. 3. Inductance L and total number of electrons in the system N_e as a function of the capacitor surface S in the case where the resonant frequency is fixed at 1 THz and the areal density of electrons is fixed at $N_e/S = 5 \times 10^{10}$ cm^{-2}. The capacitor gap is $d = 80$ nm and $\varepsilon = 12$. We have sketched possible geometries of the LC resonator in the cases where $N_e = 10$ and $N_e \gg 1$.

the resonator frequency ω_c always matched with the frequency of the quantum transition ω_{21}, one has to increase the inductance L. This is illustrated in Fig. 3, where we plot the total number of electrons N_e in the system and the inductance L as a function of the capacitance area S, with the resonant frequency of the circuit kept equal to 1 THz. The areal electronic density is taken to be $N_e/S = 5 \cdot 10^{10}$ cm^{-2}. As a starting point, we use a geometry described in Ref. [40], where the capacitor plates are shorted by a thin wire. In that geometry, $S \approx 10^2$ μm, $N_e \approx 10^5$, and L is the wire self-inductance, on the order of pH. Let us consider a capacitor gap $d = 80$ nm, with an $L_{\mathrm{QW}} = 52$-nm-thick GaAs/AlGaAs quantum well in the capacitor, as in Fig. 2(a). In this case, the intersubband transition is $\omega_{21}/2\pi = 1$ THz, with an oscillator strength $f_{21} \approx 1$ and an effective Coulomb length $L_{21} = 38$ nm. These parameters provide a Rabi splitting $2\Omega_{\mathrm{Reff}}/2\pi = 0.77$ THz that is a significant fraction of the circuit and intersubband frequencies. By using electrical lithography techniques, the lateral size of the capacitor can be shrunk to 100 nm, which corresponds to $N_e < 10$ electrons in the structure. In this case, the architecture of the inductive element must be changed. For instance, we can envision planar spiral inductances [41,42], which can provide values as high as $L \approx 1$ nH. Other possible geometries are the planar metamaterial resonators, which have recently been exploited to obtain strong coupling between quantum wells in the THz and MIR parts of the spectrum [43,44]. The increase in the size of the inductive element is a challenging task since it will generally result in increased ohmic and radiation losses. Considering the structure as a series RLC circuit, its ohmic quality factor can be written as $Q_{\mathrm{ohm}} = 1/R\sqrt{(L/C)} = \omega_c L/R$. Since L increases with the surface of the inductive element, while the resistance R increases as its length, the ohmic quality factor can actually be improved by increasing the size of the inductance. However, notice that radiation losses usually dominate in split-ring resonators operating in the THz range, and a careful design of the inductance shape is required [45].

Eventually, as the lateral size of the capacitance is reduced to submicron sizes, the electrons will start feeling the lateral confinement of the structure [46], and care must be taken to avoid depletion [47]. Note that if the surface S is reduced below L_{QW}^2, we can no longer consider the electronic system as a two-dimensional gas but rather as a quantum box [48]. In this limit, the electrons are no longer free in the plane but are quantized in all three dimensions of space. We believe that the high-frequency LC resonator can be useful for achieving the ultrastrong coupling regime even in that case, as it allows for a good spatial overlap between the oscillating electric field of the capacitor and the electronic polarization.

Clearly, the strong reduction of the capacitor volume in the quantum LC resonator allows for the realization of the ultrastrong coupling regime with a few electrons only. We are now going to show that this regime has no classical counterpart, and it opens a new field of investigation for the light-matter interaction, disclosing relevant connections between atomic physics and condensed matter. In particular, it shows the logical continuity between the Rabi Hamiltonian of atomic physics and the Hopfield Hamiltonian for condensed-matter polaritons. Moreover, the presence of the dipole-dipole interactions $\mathcal{H}_{\mathrm{P2}}$, which has been neglected so far in our discussion, brings quantitative modification of the energy spectrum of the electronic system.

Since the dipole-dipole term is also expressed from the superradiant operators in Eq. (11), $\mathcal{H}_{\mathrm{P2}} = \hbar\omega_{P1}^2/4\omega_{21}(D^+ + D^-)^2$, it acts on the very same states $|J, M\rangle$ that interact with the circuit photons. In order to derive the corresponding many-body electronic states, we shall first analyze the purely electronic part $\mathcal{H}_{\mathrm{e}} + \mathcal{H}_{\mathrm{P2}}$ of the total Hamiltonian (6) in the basis of superradiant states $|J, M\rangle$. The action of $\mathcal{H}_{\mathrm{e}} + \mathcal{H}_{\mathrm{P2}}$ in this basis is expressed as a tridiagonal matrix that can be readily diagonalized numerically (more information is provided in Appendix A). A set of results is provided in Fig. 4(a), where we plot the frequencies of the first four electronic transitions, $\omega_j - \omega_G$, $j = 1, \ldots, 4$, with $\omega_G = E_G/\hbar$ the frequency of the ground state, as a function of the total number of electrons N_e, while the electronic density N_e/S is constant and equal to $5 \cdot 10^{10}$ cm^{-2}. Using the same quantum well as for Fig. 3, we obtain from Eq. (10) the value $\omega_{P1} = 2\pi \times 1.12$ THz. In order to be able to compare systems with a constant number of electrons per unit surface, while the number of electron increases, we also must rescale the plasma frequency for each number $N_e > 1$. Since, according to Eq. (10), the one-electron plasma frequency ω_{P1} scales as $\sim 1/\sqrt{S}$, in order to perform the

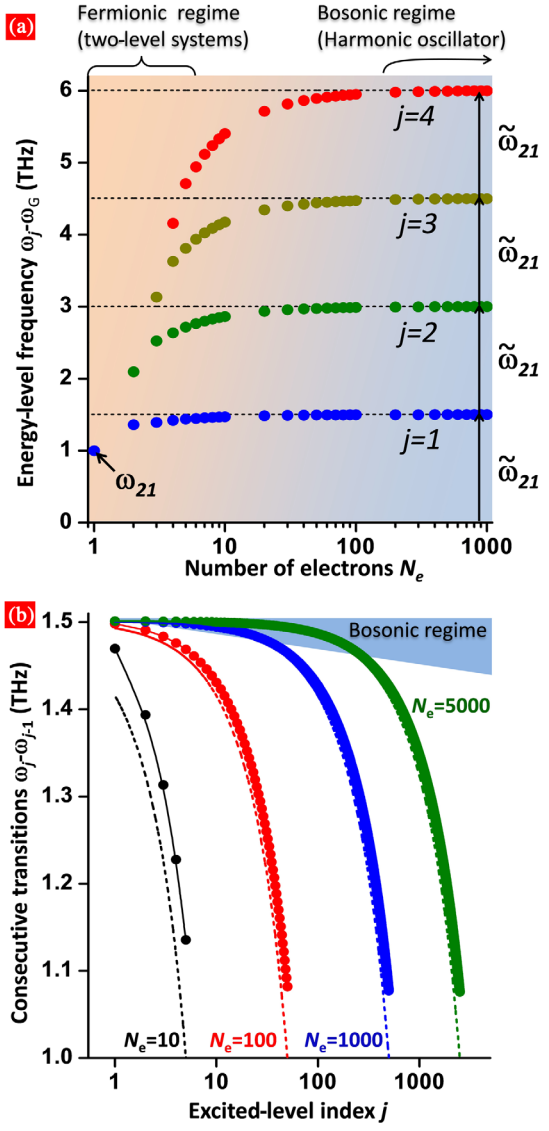

FIG. 4. (a) Frequencies of the first four many-body states of the 2DEG, above the ground state, as a function of the total number of electrons in the system N_e. The areal density is fixed at $N_e/S = 5 \times 10^{10}$ cm^{-2}. As the number of electrons is increased, the first levels become equally spaced with a separation $\tilde{\omega}_{21} = \sqrt{\omega_{21}^2 + \omega_{P1}^2 N_e}$. (b) Value of the frequency spacing $\Delta\omega_j = \omega_j - \omega_{j-1}$ as a function of the number of electrons j excited on the second subband, for different values of N_e. The dashed lines are the prediction of the formula $\tilde{\omega}_{21}(j) = \sqrt{\omega_{21}^2 + \omega_{P1}^2(N_1 - N_2)} = \sqrt{\omega_{21}^2 + \omega_{P1}^2(N_e - 2j)}$.

simulation with $N_e/S = \text{const}$, we scale down the plasma frequency according to the formula $\omega_{P1} = 1.12\omega_{21}/\sqrt{N_e}$. This scaling allows us to compare the impact of the interaction term $\mathcal{H}_{P2}$ for systems with different number of particles but with the same areal density. For simplicity, we have ignored the spin of electrons in these computations; otherwise, the states plotted in Fig. 4(a) must be considered twofold degenerate.

The results from Fig. 4(a) illustrate a radical change of the behavior of the many-body excitations of the electron gas as the number of electrons is varied. In the case of a single electron, $N_e = 1$, the depolarization term $\mathcal{H}_{P2}$ does not change the subband separation $\omega_1 - \omega_G = \omega_{21}$ (see Appendix C 1). As the number of electrons is progressively increased, the dipole-dipole interaction transfers the anharmonicity towards the high-energy states. One can see (Fig. 4) that low-energy states become equally spaced, while the energy separation between the excited levels with a high index j is reduced, thus creating a strong anharmonicity in the final part of the ladder of superradiant multielectron states $|J, M\rangle$. This is visible in Fig. 4 up to a hundred electrons. Finally, as the number of electrons becomes very high ($N_e > 1000$), we observe that the constant energy separation of the lower excited levels becomes $\omega_j - \omega_{j-1} = \tilde{\omega}_{21} = 2\pi \times 1.55$ THz, which is larger than the original transition frequency $\omega_{21} = 2\pi \times 1$ THz. The value of $\tilde{\omega}_{21}$ is well recovered by the formula $\tilde{\omega}_{21}^2 = \omega_{21}^2 + \omega_{P1}^2 N_e$ describing the depolarization shift in an intersubband system [49]. Indeed, we observe that the subspace of the first few excited states of the electronic system coincides with the spectrum of a quantum harmonic oscillator with frequency $\tilde{\omega}_{21}$. In this limit, where $N_e \gg J + M$, the electronic ensemble behaves as a composite boson, also known as the intersubband plasmon mode [35,49], described by a creation operator $p^\dagger \sim D^+/\sqrt{N_e}$ [11,15,35] (see also Appendix B), and we can replace the electronic Hamiltonian $\mathcal{H}_e + \mathcal{H}_{P2}$ with an effective bosonic Hamiltonian $\hbar\tilde{\omega}_{21} p^\dagger p$.

A similar analysis can also be performed for the excited states that lie higher above the ground state. Let us assume that there are, on average, N_1 electrons on the first subband and N_2 electrons on the second subband, with $N_1 > N_2$. Then the plasmonic picture provides an energy-level spacing of $\tilde{\omega}_{21}^2 = \omega_{21}^2 + \omega_{P1}^2(N_1 - N_2)$ [35]. This formula is numerically tested by our model in Fig. 4(b). For the excited level of index $j = J + M$, we have $N_2 = j$ electrons excited on the second subband and $N_1 - N_2 = N_e - 2j$. The plasmon picture then provides the analytical law $\omega_j - \omega_{j-1} = \sqrt{\omega_{21}^2 + \omega_{P1}^2(N_e - 2j)}$. In Fig. 4(b), we have plotted the level spacings $\omega_j - \omega_{j-1}$ as a function of j for different systems with different numbers of electrons N_e (dotted lines). We observe that, when N_e becomes sufficiently large, then $\omega_j - \omega_{j-1}$ is well described by the formula $\sqrt{\omega_{21}^2 + \omega_{P1}^2(N_e - 2j)}$ for up to 10% of the excited levels. The range of energies where the bosonization can be applied also expands with N_e [the "bosonic regime," shaded region in Fig. 4(b)]. This behavior has been confirmed in experiments with intersubband systems, where $N_1 - N_2$ is varied through temperature, applied bias, or interband pump [50–52].

Our model is then able to quantitatively track how the bosonization of the excited states occurs as the number of

electrons in the system increases. For a low number of electrons, $N_e \lesssim 10$, we recover a pseudo-Dicke ladder with unequal level spacings that are renormalized by the dipole-dipole interactions $\mathcal{H}_{P2}$. In the limit, $N_e \gg 1$, these interactions create a collective plasmon mode with a harmonic spectrum and a renormalized energy $\hbar\tilde{\omega}_{21}$. In these two limits, the circuit-matter interactions have a different nature, and the ultrastrong coupling regime where $2\Omega_R/\omega_{21} \sim 1$ will have a different manifestation.

We now consider the full Hamiltonian from Eq. (6) and explore the behavior of the circuit-mater coupled states as the number of electrons is changed. We first compare the bosonic limit, $N_e \gg 1$, with the single-electron limit, $N_e = 1$. In the case $N_e \gg 1$, the lowest-energy excitations of the gas are described by a composite boson, which couples to the circuit photon through an effective interaction term $\mathcal{H}_{\rm int} = i\hbar\Omega_R\sqrt{N_e}\sqrt{\omega_c/\tilde{\omega}_{21}}(p^\dagger + p)(a^\dagger - a)$ (see Appendixes B and C 2). The circuit-matter interaction is then described as the coupling between two harmonic oscillators, and we recover the polariton Hopfield model that is well known in solid-state physics [24]. Instead, in the single-electron case, we recover the Rabi model describing a two-level system coupled to a harmonic oscillator (the circuit resonator) [21,22]. In the limit where $\Omega_{R,\rm eff}/\omega_{21} \ll 1$, the antiresonant terms of the quantum Hamiltonian can be neglected, and we recover the Jaynes-Cummings model widely used in quantum optics [23]. The system depicted in Fig. 2(a) then becomes very similar to a single superconducting qubit coupled to an LC circuit or transmission line in the GHz range [7,8].

These two limits are illustrated in Fig. 5, when the system is pushed in the ultrastrong coupling regime with a circuit-matter coupling constant $2\Omega_{R,\rm eff} = \Omega_R\sqrt{N_e} = 0.77\omega_{21}$ that is identical in both cases. In this figure, we compare the dispersion of the coupled states when $N_e \gg 1$ (a) and $N_e = 1$ (b). These plots are obtained by computing the linear response of the circuit under a weak harmonic bias $V(t) = V_0\cos(\omega t)$ [36] (Appendix C). The circuit frequency ω_c is swept around the frequency of the intersubband transition $\omega_{21} = 2\pi \times 1$ THz. We can envision, for instance, that the THz oscillating voltage is applied to the system through a nano-antenna [53,54]. When $N_e \gg 1$ [Fig. 5(a)], we have considered two coupled quantum harmonic oscillators with frequencies ω_c and $\tilde{\omega}_{21}$ [35] (see Appendix C 2). In this case, we observe in the spectra only two normal modes, the polaritons, split by an energy $2\hbar\Omega_{R,\rm eff}$ when the resonance condition $\omega_c = \tilde{\omega}_{21}$ is met. The ultrastrong coupling makes the opening of a gap in the dispersion curve of the polaritons [15,25] evident.

The same plot, performed for the case $N_e = 1$, presents completely different features. In this case, our Hamiltonian (6) is reduced to a Rabi-like model of the two-level system depicted in Fig. 5(b) (see Appendix C 1). Now the resonant condition is $\omega_c = \omega_{21}$, and there is no gap opening in the dispersion of the coupled states. However, since the coupling constant Ω_R is a significant value of the transition frequency, the Jaynes-Cummings approximation does not hold and the Hamiltonian must be solved together with the nonresonant terms in $\mathcal{H}_{\rm int}$ [Eq. (7)]. These terms induce couplings of the ground state with the higher-order dressed states of the system [33] (Appendix C 1). They manifest by the appearance of additional peaks in the transmission spectra, as indicated in Fig. 5(b). In particular, the antiresonant terms also render the splitting visible between the dressed states with, respectively, two and three photons. Note that this splitting, $2\Omega_R\sqrt{2} = 2\pi \times 1$, 1 THz, is, in the present case, higher than the frequency of the two-level system, ω_{21}. Recently, similar ultrastrong coupling effects have been extensively studied in the framework of the Rabi model [55].

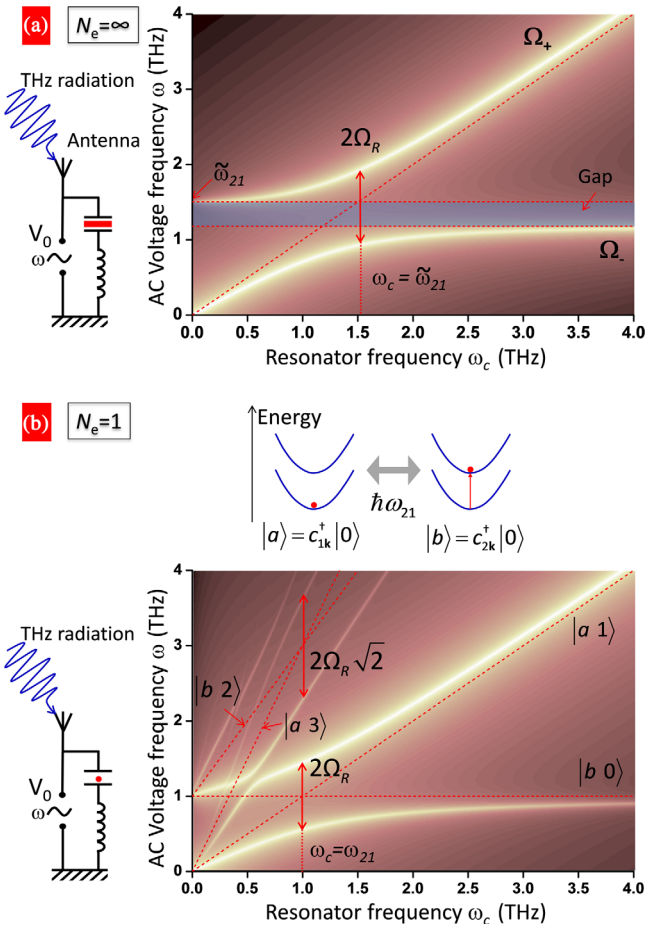

FIG. 5. (a) Absorption spectrum of an LC circuit coupled with the 2DEG of the quantum well. The vertical (y) axis is the frequency of the probing voltage, the horizontal (x) axis is the frequency of the resonator ω_c, and the color code (z axis) is the strength of the absorption signal, on a logarithmic scale. Details of the computation are provided in Appendix C 2. In this case, the circuit is coupled with the intersubband plasmon mode, and the typical anticrossing curves are seen. For this plot, the circuit-matter coupling constant is $2\Omega_{R,\rm eff} = 0.77\omega_{21}$. (b) The same plot obtained for the case of a single electron in the capacitor, as obtained from the Rabi model (Appendix C 1).

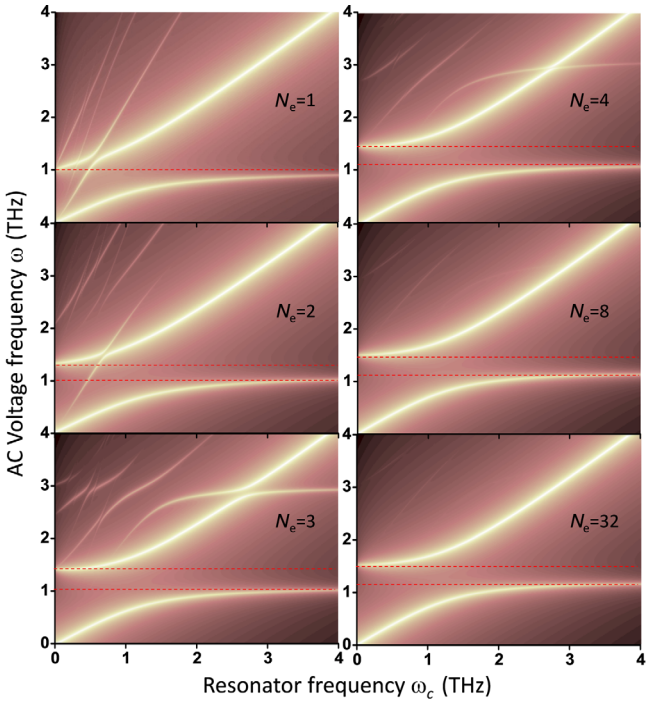

FIG. 6. Absorption spectra of the coupled circuit-matter system with a variable number of electrons N_e. The parameters for these plots are identical to those in Fig. 5.

Our model also allows us to explore the crossover between the fermionic and bosonic ultrastrong light-matter coupling regimes as the capacitor surface is increased. In Fig. 6, we provide plots of the absorption of the system obtained by applying the small voltage probe, as the number of electrons participating in the interaction with light is progressively augmented. We observe that the high-order dressed levels are visible up to $N_e = 4$ electrons in the capacitor core. However, beyond that number, the quantum nonlinearities due to the fermionic nature of the material excitations are rapidly washed away until we observe only two polariton branches that are identical to the ones obtained from the coupled-oscillator model. The forbidden gap between the polariton states is almost identical to the one already observed in the $N_e = 2$ case in Fig. 6. Yet, for that case, the gap is not strict since we still observe a weak mixing between the one- and three-photon dressed states as in the $N_e = 1$ case and in Fig. 5(b).

IV. CONCLUSION

In this paper, we have described how the ultrastrong light-matter coupling, which has been demonstrated in many-electron systems, evolves in a regime where the high concentration is preserved but only a few electrons remain. To envision such a system, it is necessary to enormously reduce the volume in which light-matter interaction takes place and go far below the limit of diffraction. This is possible within the capacitor of a circuit that is described by lumped elements, like an *LC* circuit. We have shown that the problem is formally similar to the case of microcavities, even though in the case of an *LC* resonator, the coupling does not occur through cavity photons but rather with circuit photons that interact with a resonant polarization.

In this context, we have studied the ultrastrong light-matter interaction down to the limit of one electron only. In particular, we have investigated the effect due to the quadratic polarization term of the electromagnetic Hamiltonian which is at the origin of the collective phenomena when a multitude of electrons are present. This term radically changes the spectrum and has a more significant impact on the system with a few delocalized electrons than for an ensemble of spatially localized atoms. The main reason for this strong effect is because the electronic wave functions in condensed matter highly overlap and can give rise to a much stronger dipole-dipole interaction than for atoms in distinct positions of the space. In particular, in the limit of a few electrons, the absorption frequency of our system is strongly dependent on the number of excitations [Fig. 4(a)]. We therefore believe that the proposed device architecture could be suitable for the implementation of fascinating quantum-optical phenomena, such as nonlinear optics on a single-photon level [56,57]. Note that these results were obtained at the lowest dipole-dipole order of the Coulomb interaction, while higher-order effects could be responsible for phenomena such as stimulated scattering of lasing [58]. Furthermore, we show that by using the base of superradiant Dicke states, we can connect the fermionic few-electron Rabi model to the bosonic Hopfield Hamiltonian and observe the rapid emergence of the collective plasma excitations with the increasing number of electrons coupled to the light.

The system described could also be interesting for quantum-information processing [59]. In the limit of a few electrons, our *LC* circuit shows similar features to those well known in atomic physics described by quantum electrodynamics. Furthermore, this approach could be an alternative to superconducting circuits in order to insert quantum functions in condensed-matter devices. Owing to the strong dipole-dipole interactions, our system could also be interesting for implementing quantum-information-processing protocols, similar to the ones proposed for cold Rydberg atoms [59]. This aspect could be particularly relevant in the case of few-electron systems that operate like quantum "qudits" [60,61], where the dimension of the quantum bit is fixed by the number of electrons N_e. In the context of semiconductor heterostructures, the particle-particle interaction can be tailored by wave-function engineering and carrier depletion by an external gate [51,62]. In such quantum devices operating in the few-electron limit, the superradiant states, ultrastrongly coupled to the circuit photon, can be injected by direct tunneling, thus opening the possibility to read out quantum electrodynamical properties via the measure of a DC current.

ACKNOWLEDGMENTS

The authors acknowledge financial support from the European Research Council grant "ADEQUATE."

APPENDIX A: ELECTRONIC HAMILTONIAN MATRIX ELEMENTS

The matter part of the Hamiltonian of our system is expressed by the superradiant operators as

$$\mathcal{H}_e + \mathcal{H}_{P2} = \sum_{\mathbf{k}} (\hbar\omega_{1\mathbf{k}} c_{1\mathbf{k}}^\dagger c_{1\mathbf{k}} + \hbar\omega_{2\mathbf{k}} c_{2\mathbf{k}}^\dagger c_{2\mathbf{k}}) + \frac{\hbar\omega_{P1}^2}{4\omega_{21}} (D^+ + D^-)^2. \tag{A1}$$

Here, D^+ and D^- are provided by Eq. (11). We seek to diagonalize this Hamiltonian in the basis of superradiant states spanned by the successive application of the operator D^+ on the fundamental state $|F\rangle = \prod_{|\mathbf{k}|\leq k_F} c_{1\mathbf{k}}^\dagger |0\rangle$:

$$|J, M\rangle = \sqrt{\frac{(J-M)!}{N_e!(J+M)!}} (D^+)^{J+M} |F\rangle. \tag{A2}$$

We remind the reader that the state $|JM\rangle$ is a symmetric linear superposition of all states with $J+M$ excited electrons on the second subband. In this representation, the ground state is expressed as $|F\rangle = |J, -J\rangle$. Using the commutation relation $[\mathcal{H}_e, D^\pm] = \pm\hbar\omega_{21} D^\pm$ and Eq. (A2), it is easy to show that $|J, M\rangle$ is an eigenstate of the kinetic Hamiltonian $\mathcal{H}_e$:

$$\mathcal{H}_e |J, M\rangle = [E_G + \hbar\omega_{21}(J+M)] |J, M\rangle. \tag{A3}$$

The action of the depolarization (dipole-dipole) part is also readily computed with the relations [39]

$$D^+ |J, M\rangle = \sqrt{J(J+1) - M(M+1)} |J, M+1\rangle, \tag{A4}$$

$$D^- |J, M\rangle = \sqrt{J(J+1) - M(M-1)} |J, M-1\rangle. \tag{A5}$$

The Hamiltonian (A1) is then written in this basis $|J, M\rangle$ as a symmetric tridiagonal matrix:

$$\langle j | \mathcal{H}_e + \mathcal{H}_{P2} | j \rangle = E_G + j\hbar\omega_{21} + \frac{\hbar\omega_{P1}^2}{4\omega_{21}} [(2j+1)N_2 - 2j^2], \tag{A6}$$

$$\langle j | \mathcal{H}_e + \mathcal{H}_{P2} | j+2 \rangle = \langle j+2 | \mathcal{H}_e + \mathcal{H}_{P2} | j \rangle = \frac{\hbar\omega_{P1}^2}{4\omega_{21}} \sqrt{(j+1)(N_e - j)(j+2)(N_e - 1 - j)}, \tag{A7}$$

which is diagonalized numerically. Here, $j = J + M$ is the number of electrons excited on the second subband, and $|j\rangle = |J, M\rangle$.

APPENDIX B: BOSONIZATION

In this section, we provide a justification for the numerical results in Figs. 4(a) and 4(b), which show that for a very large number of electrons in the system, the quasiparticle excitations behave as bosons. For this, we start with the commutators of the operators D^+ and D^- with the number operators $\hat{N}_1 = \sum_{\mathbf{k}} c_{1\mathbf{k}}^\dagger c_{1\mathbf{k}}$ and $\hat{N}_2 = \sum_{\mathbf{k}} c_{2\mathbf{k}}^\dagger c_{2\mathbf{k}}$:

$$[D^+, D^-] = \hat{N}_1 - \hat{N}_2, \tag{B1}$$

$$[D^\pm, \hat{N}_1 - \hat{N}_2] = 0. \tag{B2}$$

These commutation rules mean that the operator $\hat{N}_1 - \hat{N}_2$ behaves as the identity operator in the subspace where the difference $\Delta N = N_1 - N_2$ is fixed. This remains approximately true if the system contains a large number of electrons and evolves in a subspace where the variations of ΔN are small. Furthermore, if we suppose that the system is below the transparency region $\Delta N > 0$, we can define (almost) bosonic operators $b^\dagger$ and b:

$$b^\dagger = \frac{1}{\sqrt{\Delta N}} D^+, \qquad b = \frac{1}{\sqrt{\Delta N}} D^-, \tag{B3}$$

$$[b, b^\dagger] = 1. \tag{B4}$$

This result can also be obtained in a more formal way by using a Holstein-Primakoff transformation in the thermodynamic limit $N_1 \to \infty$ [63]. Note, however, that this transformation cannot be provided in a closed form in the general case of a finite number of electrons because of the presence of D^{+2} and D^{-2} terms in the interaction Hamiltonian from Eq. (A1). We can therefore reexpress the Hamiltonian (A1) in the limit with a very large number of electrons [35]:

$$\mathcal{H}_e + \mathcal{H}_{P2} = \hbar\omega_{21} b^\dagger b + \frac{\hbar\omega_{P1}^2 \Delta N}{4\omega_{21}} (b^\dagger + b)^2. \tag{B5}$$

In the above equation, the kinetic part of the electronic Hamiltonian $\mathcal{H}_e$ is replaced by an effective bosonic term $\hbar\omega_{21} b^\dagger b$, which yields the same evolution of the excited states. This Hamiltonian can be diagonalized with a Hopfield-Bogoliubov transformation to yield [15,35]

$$\mathcal{H}_e + \mathcal{H}_{P2} = \hbar\tilde{\omega}_{21} p^\dagger p, \quad \tilde{\omega}_{21} = \sqrt{\omega_{21}^2 + \omega_{P1}^2 \Delta N}. \tag{B6}$$

Here, $p^\dagger$ and p are new bosonic operators that describe the intersubband plasmon mode with a frequency $\tilde{\omega}_{21}$, which is equivalent to a quantum harmonic oscillator. This

is exactly the result presented, for instance, in Fig. 4(a), where $\Delta N \approx N_1 \approx N_e$.

APPENDIX C: RESPONSE TO APPLIED VOLTAGE IN THE LINEAR REGIME

In order to obtain the absorption spectra of the system, as presented in Figs. 5 and 6, we add to the total Hamiltonian a weak harmonic perturbation [36]:

$$\mathcal{H}_{\text{pert}} = \frac{\hbar V_0 \cos(\omega t)}{\sqrt{2\hbar Z}}(a + a^\dagger). \tag{C1}$$

The energy absorbed by the system, averaged over a unit cycle, is then expressed as

$$\frac{d\bar{U}}{dt}(\omega) = \frac{\omega\pi}{4}\frac{V_0^2}{Z}\int_{-\infty}^{\infty} C_{AA}(t)e^{i\omega t}dt. \tag{C2}$$

Here, $C_{AA}(t) = \langle A_I(t)A_I(0)\rangle$ is the autocorrelation function of the perturbation $A = a^\dagger + a$, and the subscript "I" means that the corresponding operator is expressed in the interaction picture. The average is computed on the eigenstates of the unperturbed Hamiltonian [64]. If the system is at $T = 0$ K and initially in its ground state $|G\rangle$, then we have

$$C_{AA}(t) = \sum_E |\langle E|(a^\dagger + a)|G\rangle|^2 e^{i\omega_{EG}t}. \tag{C3}$$

Here, $|E\rangle$ is an excited state of the system, and $\omega_{EG} = \omega_E - \omega_G$ is its frequency with respect to the ground state. Including phenomenological damping factors Γ that describe dissipation and performing the integral in Eq. (C2), we obtain the energy-loss spectra of the system:

$$\frac{d\bar{U}}{dt}(\omega) = \frac{\pi V_0^2}{Z}\sum_E \frac{Q_E\Gamma^2/4}{(\omega-\omega_{EG})^2 + \Gamma^2/4}|\langle E|(a^\dagger + a)|G\rangle|^2. \tag{C4}$$

Here, we introduced the quality factor $Q_E = \omega_{EG}/\Gamma$ of the excited state. Take, as an example, a harmonic oscillator with a Hamiltonian $\mathcal{H} = \hbar\omega_0(a^\dagger a + 1/2)$; then, Eq. (C4) provides a single absorption peak at the frequency ω_0, as expected.

1. The case of one electron: The Rabi model

Let us first consider the case where there is just one electron in the system, $N_e = 1$. We consider that the electron occupies the $\mathbf{k} = 0$ state, and we drop the wave-vector indices. The electronic Hamiltonian (A1) becomes

$$\mathcal{H}_e + \mathcal{H}_{P2} = \hbar\omega_1\hat{N}_1 + \hbar\omega_2\hat{N}_2 + \frac{\hbar\omega_{P1}^2}{4\omega_{21}}(c_2^\dagger c_1 + c_1^\dagger c_2)^2. \tag{C5}$$

Here, $\hat{N}_j = c_j^\dagger c_j$, and the single electron evolves between the two states $c_1^\dagger|0\rangle$ and $c_2^\dagger|0\rangle$. Using Eqs. (A6) and (A7) for the states $j = 0$ and $j = 1$ with $N_e = 1$, one can show that the quadratic term induces only a shift of the bare subband energies, and therefore, one can replace Eq. (C5) with an effective Hamiltonian:

$$\mathcal{H}_e + \mathcal{H}_{P2} = \hbar\bar{\omega}_1\hat{N}_1 + \hbar\bar{\omega}_2\hat{N}_2, \tag{C6}$$

$$\bar{\omega}_{1,2} = \omega_{1,2} + \frac{\omega_{P1}^2}{4\omega_{21}}. \tag{C7}$$

The full Hamiltonian of the system, including light-matter coupling, then becomes

$$\mathcal{H} = \hbar\bar{\omega}_1\hat{N}_1 + \hbar\bar{\omega}_2\hat{N}_2 + i\hbar\Omega_R\sqrt{\frac{\omega_c}{\omega_{21}}}(c_2^\dagger c_1 + c_1^\dagger c_2)(a^\dagger - a). \tag{C8}$$

This Hamiltonian corresponds to a Rabi model [21] with a light-matter coupling constant $\Xi = \Omega_R\sqrt{\omega_c/\omega_{21}}$. Usually, this model is simplified to the Jaynes-Cummings Hamiltonian by excluding the antiresonant terms in Eq. (C8); however, since we are interested in the ultrastrong coupling effects, we will not use this approximation. The Hamiltonian (C8) is numerically diagonalized on the basis of dressed states $c_{1,2}^\dagger|0,n\rangle$, where $|0\rangle$ stands for the electronic vacuum and $|n\rangle$ is a Fock state of n photons. The Hamiltonian (C8) acts separately on two subspaces, which can be dubbed "resonant" $\mathcal{R}$ and "antiresonant" $\mathcal{A}$ subspaces:

$$\mathcal{R} = \{c_2^\dagger|0,2k\rangle, c_1^\dagger|0,2k+1\rangle\}, \tag{C9}$$

$$\mathcal{A} = \{c_1^\dagger|0,2k\rangle, c_2^\dagger|0,2k+1\rangle\}. \tag{C10}$$

We have

$$\frac{\mathcal{H}}{\hbar}\Big|_{\mathcal{R}} = \begin{array}{c} \begin{array}{ccccc} c_2^\dagger|0,0\rangle & c_1^\dagger|0,1\rangle & c_2^\dagger|0,2\rangle & c_1^\dagger|0,3\rangle & \cdots \end{array} \\ \begin{pmatrix} \bar{\omega}_2 & -i\Xi & 0 & 0 & \cdots \\ i\Xi & \bar{\omega}_1+\omega_c & -i\Xi\sqrt{2} & 0 & \cdots \\ 0 & i\Xi\sqrt{2} & \bar{\omega}_2+2\omega_c & -i\Xi\sqrt{3} & \cdots \\ 0 & 0 & i\Xi\sqrt{3} & \bar{\omega}_1+3\omega_c & \cdots \\ \vdots & \vdots & \vdots & \vdots & \ddots \end{pmatrix} \end{array}, \tag{C11}$$

$$\frac{\mathcal{H}}{\hbar}\Big|_{\mathcal{A}} = \begin{array}{c} \begin{matrix} c_1^\dagger|0,0\rangle & c_2^\dagger|0,1\rangle & c_1^\dagger|0,2\rangle & c_2^\dagger|0,3\rangle & \cdots \end{matrix} \\ \begin{Bmatrix} \bar{\omega}_1 & -i\Xi & 0 & 0 & \cdots \\ i\Xi & \bar{\omega}_2+\omega_c & -i\Xi\sqrt{2} & 0 & \cdots \\ 0 & i\Xi\sqrt{2} & \bar{\omega}_1+2\omega_c & -i\Xi\sqrt{3} & \cdots \\ 0 & 0 & i\Xi\sqrt{3} & \bar{\omega}_2+3\omega_c & \cdots \\ \vdots & \vdots & \vdots & \vdots & \ddots \end{Bmatrix} \end{array}. \tag{C12}$$

Note that these subspaces differ only by the permutation of the subband indices 1 and 2. This is not astonishing since Eq. (C8) preserves its formal expression upon this permutation. The two subspaces $\mathcal{R}$ and $\mathcal{A}$ yield two distinct sets of eigenvalues and eigenstates:

$$\omega_\rho, \quad |\rho\rangle = \sum_{k\geq 0}(x_k^\rho c_2^\dagger|0,2k\rangle + y_k^\rho c_1^\dagger|0,2k+1\rangle), \tag{C13}$$

$$\omega_\alpha, \quad |\alpha\rangle = \sum_{k\geq 0}(z_k^\alpha c_1^\dagger|0,2k\rangle + t_k^\alpha c_2^\dagger|0,2k+1\rangle). \tag{C14}$$

Here, ω_ρ and ω_α are the eigenvalues of the matrices (C11) and (C12), respectively. The fundamental lowest-energy state of the system is provided by the lowest-energy eigenvector in the antiresonant subspace $\mathcal{A}$, $|\alpha_0\rangle$, with an eigenfrequency ω_{α_0}. In the absence of photons, this state has a frequency $\omega_{\alpha_0} = \bar{\omega}_1$, and $|\alpha_0\rangle = c_1^\dagger|0,0\rangle$. The coupling with light renormalizes this value, as the state $c_1^\dagger|0,0\rangle$ is now coupled to all the dressed states in $\mathcal{A}$, as can be seen from Eq. (C12).

Let us now apply the linear response theory. We suppose that the system is initially in its ground state $|\alpha_0\rangle$. Furthermore, it is easy to show that the perturbation $A = a^\dagger + a$ does not couple states within the same subspace $\mathcal{R}$ or $\mathcal{A}$. Therefore, this perturbation induces only transitions between the new ground state $|\alpha_0\rangle$ and all the states in $\mathcal{R}$. The measured spectrum of the system is then

$$\frac{d\bar{U}}{dt}(\omega) = \frac{\pi V_0^2 Q}{Z}\sum_\rho \frac{\Gamma^2/4}{(\omega-\omega_{\rho\alpha_0})^2+\Gamma^2/4}|C_{\rho\alpha_0}|^2. \tag{C15}$$

Here, we have defined

$$C_{\rho\alpha_0} = \sum_{k\geq 0}(x_k^{\rho *} t_k^{\alpha_0} + y_k^{\rho *} z_k^{\alpha_0})\sqrt{2k+1}, \tag{C16}$$

and we have supposed for simplicity that all the transitions share the same quality factor Q.

To grasp the meaning of these equations, let us consider the case where the LC circuit is tuned in resonance with the intersubband transition, $\omega_{21} = \bar{\omega}_2 - \bar{\omega}_1 = \omega_c$, and the light-matter coupling constant Ξ is sufficiently small so that the Jaynes-Cumming approximation can be applied. Since the antiresonant terms are neglected, we have $|\alpha_0\rangle = c_1^\dagger|0,0\rangle$ and $z_k^{\alpha_0} = \delta_{0k}$ and $t_k^{\alpha_0} = 0$ from Eq. (C12). Furthermore, Eq. (C11) breaks into a block-diagonal matrix, each block corresponding to a pair of quasiresonant states $c_2^\dagger|0,2k\rangle$ and $c_1^\dagger|0,2k+1\rangle$. The only contributions in the sum (C15) will therefore arise from the eigenstates $|\rho_\pm\rangle = x_\pm c_2^\dagger|0,0\rangle + y_\pm c_1^\dagger|0,1\rangle$ that are solutions of the secular equation:

$$\begin{Bmatrix} \bar{\omega}_2 & -i\Xi \\ i\Xi & \bar{\omega}_1+\omega_c \end{Bmatrix}\begin{Bmatrix} x_\pm \\ y_\pm \end{Bmatrix} = \omega_\pm \begin{Bmatrix} x_\pm \\ y_\pm \end{Bmatrix}. \tag{C17}$$

Then, the spectrum described by Eq. (C15) appears as two peaks that correspond to these two photon-electron coupled states.

If, on the contrary, the light-matter constant Ω_R is a significant fraction of the transition energy ω_{21} so that the system is in the "ultrastrong" coupling regime, then the fundamental state of the system contains contributions from the high-energy states in the antiresonant subspace $\mathcal{A}$, and respectively, the spectrum (C15) will contain peaks that arise from the high-energy states of the resonant subspace $\mathcal{R}$.

2. The case of many electrons: Intersubband plasmon polaritons in the Hopfield model

Let us consider the case where the system evolves not very far from the ground state, where almost all electrons fill the first subband $N_1 \approx N_e \gg N_2$ and $\Delta N \approx N_e$. The bosonized Hamiltonian of the system can then be written as [15,35]

$$\mathcal{H} = \hbar\omega_c(a^\dagger a + 1/2) + \hbar\tilde{\omega}_{21}p^\dagger p + i\hbar\Omega_{R\text{eff}}\sqrt{\frac{\omega_c}{\tilde{\omega}_{21}}}(a^\dagger - a)(p^\dagger + p). \tag{C18}$$

We recall that the effective coupling constant is $\Omega_{R\text{eff}} = \Omega_R\sqrt{N_e}$, with Ω_R provided by Eq. (9). This Hamiltonian describes two coupled quantum oscillators and can be diagonalized to

$$\mathcal{H} = \hbar W_+ \Pi_+^\dagger \Pi_+ + \hbar W_- \Pi_-^\dagger \Pi_-. \tag{C19}$$

Here, $W_\pm$ are the frequencies of the two polariton modes that are solutions of the secular equation:

$$(W_\pm^2 - \tilde{\omega}_{21}^2)(W_\pm^2 - \omega_c^2) = 4\Omega_{R\text{eff}}^2\tilde{\omega}_{21}\omega_c, \tag{C20}$$

which can be solved exactly. Furthermore, the operators $\Pi_\pm^\dagger$ are expressed as a function of the old ones:

$$\Pi_\pm^\dagger = x_\pm a^\dagger + y_\pm a + z_\pm p^\dagger + t_\pm p. \tag{C21}$$

Here, the Hopfield coefficients x, y, z, and t can be expressed analytically if necessary. In order to obtain the spectrum of the system, we need to compute the matrix elements of the perturbation $A = a^\dagger + a$ between the excited states $|E\rangle$ and the ground state $|G\rangle$ of the Hamiltonian (C18). The excited state can have any number of polariton excitations n created by the operators $\Pi_\pm^\dagger$:

$$|E\rangle = \frac{1}{\sqrt{n!}}(\Pi_\pm^\dagger)^n|G\rangle, \tag{C22}$$

and any linear combination of states like in Eq. (C22) is an excited state. The ground state $|G\rangle$ itself can be expressed with an infinite linear combination of operators a, $a^\dagger$, p, and $p^\dagger$ acting on the uncoupled ground state $|F\rangle|n=0\rangle$, and it cannot be provided in an analytical closed form exactly. Nevertheless, the spectrum of the system from Eq. (C2) can be provided in a closed form. We first show that the perturbation $a^\dagger + a$ can only couple single plasmon states $\Pi_\pm^\dagger|G\rangle$ with the ground state $|G\rangle$. For this, we note that

$$\begin{aligned}\langle G|a(\Pi_\pm^\dagger)^n|G\rangle &= \langle G|[a,\Pi_\pm^\dagger](\Pi_\pm^\dagger)^{n-1}|G\rangle \\ &\quad + \langle G|\Pi_\pm^\dagger a(\Pi_\pm^\dagger)^{n-1}|G\rangle.\end{aligned} \tag{C23}$$

The second term in the above equation is zero since $\langle G|\Pi_\pm^\dagger = (\Pi_\pm|G\rangle)^\dagger = 0$. Using Eq. (C21), the first term is reduced to

$$\langle G|[a,\Pi_\pm^\dagger](\Pi_\pm^\dagger)^{n-1}|G\rangle = x_\pm\langle G|(\Pi_\pm^\dagger)^{n-1}|G\rangle = x_\pm\delta_{1,n}, \tag{C24}$$

which completes our proof. A similar result is valid for $a^\dagger$. As a result, contrary to the previous section, the spectrum of the system is composed of only two absorption peaks, centred around the polariton frequencies $W_\pm$:

$$\begin{aligned}\frac{d\bar{U}}{dt}(\omega) &= \frac{\pi V_0^2 Q}{Z} \\ &\quad \times \left(\frac{|x_+ - y_+|^2\Gamma^2/4}{(\omega - W_+)^2 + \Gamma^2/4} + \frac{|x_- - y_-|^2\Gamma^2/4}{(\omega - W_-)^2 + \Gamma^2/4}\right).\end{aligned} \tag{C25}$$

This equation corresponds to the plot of Fig. 5(a).

[1] Y. Yamamoto, F. Tassone, and H. Cao, *Semiconductor Cavity Quantum Electrodynamics* (Springer-Verlag, Berlin, 2000).

[2] R. J. Thompson, G. Rempe, and H. J. Kimble, *Observation of Normal-Mode Splitting for an Atom in an Optical Cavity*, Phys. Rev. Lett. **68**, 1132 (1992).

[3] M. Brune, F. Schmidt-Kaler, A. Maali, J. Dreyer, E. Hagley, J. M. Raimond, and S. Haroche, *Quantum Rabi Oscillation: A Direct Test of Field Quantization in a Cavity*, Phys. Rev. Lett. **76**, 1800 (1996).

[4] C. Weisbuch, M. Nishioka, A. Ishikawa, and Y. Arakawa, *Observation of the Coupled Exciton-Photon Mode Splitting in a Semiconductor Quantum Microcavity*, Phys. Rev. Lett. **69**, 3314 (1992).

[5] J. P. Reithmaier, G. Sek, A. Löffler, C. Hofmann, S. Kuhn, S. Reitzenstein, L. V. Keldysh, V. D. Kulakovskii, T. L. Reinecke, and A. Forchel, *Strong Coupling in a Single Quantum Dot-Semiconductor Microcavity System*, Nature (London) **432**, 197 (2004).

[6] T. Yoshie, A. Scherer, J. Hendrickson, G. Khitrova, H. M. Gibbs, G. Rupper, C. Ell, O. B. Shchekin, and D. G. Deppe, *Strong Coupling in a Single Quantum Dot-Semiconductor Microcavity System*, Nature (London) **432**, 200 (2004).

[7] I. Chiorescu, P. Bertet, K. Semba, Y. Nakamura, C. J. P. M. Harmans, and J. E. Mooij, *Coherent Dynamics of a Flux Qubit Coupled to a Harmonic Oscillator*, Nature (London) **431**, 159 (2004).

[8] A. Wallraff, D. I. Schuster, A. Blais, L. Frunzio, R.-S. Huang, J. Majer, S. Kumar, S. M. Girvin, and R. J. Schoelkopf, *Strong Coupling of a Single Photon to a Superconducting Qubit Using Circuit Quantum Electrodynamic*, Nature (London) **431**, 162 (2004).

[9] A. A. Abdumalikov, O. Astafiev, Y. Nakamura, Y. A. Pashkin, and J. S. Tsai, *Vacuum Rabi Splitting Due to Strong Coupling of a Flux Qubit and a Coplanar-Waveguide Resonator*, Phys. Rev. B **78**, 180502 (2008).

[10] J. D. Teufel, D. Li, M. S. Allman, K. Cicak, A. J. Sirois, J. D. Whittaker, and R. W. Simmonds, *Coherent Dynamics of a Flux Qubit Coupled to a Harmonic Oscillator*, Nature (London) **471**, 204 (2011).

[11] C. Ciuti, G. Bastard, and I. Carusotto, *Quantum Vacuum Properties of the Intersubband Cavity Polariton Field*, Phys. Rev. B **72**, 115303 (2005).

[12] D. Hagenmüller, S. De Liberato, and C. Ciuti, *Ultrastrong Coupling between a Cavity Resonator and the Cyclotron Transition of a Two-Dimensional Electron Gas in the Case of an Integer Filling Factor*, Phys. Rev. B **81**, 235303 (2010).

[13] B. Peropadre, P. Forn-Díaz, E. Solano, and J. J. García-Ripoll, *Switchable Ultrastrong Coupling in Circuit QED*, Phys. Rev. Lett. **105**, 023601 (2010).

[14] A. A. Anappara, S. De Liberato, A. Tredicucci, C. Ciuti, G. Biasiol, L. Sorba, and F. Beltram, *Signatures of the Ultrastrong Light-Matter Coupling Regime*, Phys. Rev. B **79**, 201303(R) (2009).

[15] Y. Todorov, A. M. Andrews, R. Colombelli, S. De Liberato, C. Ciuti, P. Klang, G. Strasser, and C. Sirtori, *Ultrastrong Light-Matter Coupling Regime with Polariton Dots*, Phys. Rev. Lett. **105**, 196402 (2010).

[16] M. Geiser, F. Castellano, G. Scalari, M. Beck, L. Nevou, and Jérôme Faist, *Ultrastrong Coupling Regime and Plasmon Polaritons in Parabolic Semiconductor Quantum Wells*, Phys. Rev. Lett. **108**, 106402 (2012).

[17] A. Delteil, A. Vasanelli, Y. Todorov, C. Feuillet Palma, M. Renaudat St-Jean, G. Beaudoin, I. Sagnes, and C. Sirtori, *Charge-Induced Coherence between Intersubband Plasmons in a Quantum Structure*, Phys. Rev. Lett. **109**, 246808 (2012).

[18] G. Scalari, C. Maissen, D. Turcinková, D. Hagenmüller, S. De Liberato, C. Ciuti, C. Reichl, D. Schuh, W. Wegscheider, M. Beck, and J. Faist, *Ultrastrong Coupling of the Cyclotron Transition of a 2D Electron Gas to a THz Metamaterial*, Science **335**, 1323 (2012).

[19] T. Niemczyk, F. Deppe, H. Huebl, E. P. Menzel, F. Hocke, M. J. Schwarz, J. J. Garcia-Ripoll, D. Zueco, T. Hümmer, E. Solano, A. Marx, and R. Gross, *Circuit Quantum Electrodynamics in the Ultrastrong-Coupling Regime*, Nat. Phys. **6**, 772 (2010).

[20] T. Schwartz, J. A. Hutchison, C. Genet, and T. W. Ebbesen, *Reversible Switching of Ultrastrong Light-Molecule Coupling*, Phys. Rev. Lett. **106**, 196405 (2011).

[21] I. I. Rabi, *Space Quantization in a Gyrating Magnetic Field*, Phys. Rev. **51**, 652 (1937).

[22] D. Braak, *Integrability of the Rabi Model*, Phys. Rev. Lett. **107**, 100401 (2011).

[23] E. T. Jaynes and F. W. Cummings, *Comparison of Quantum and Semiclassical Radiation Theories with Application to the Beam Maser*, Proc. IEEE **51**, 89 (1963).

[24] J. J. Hopfield, *Theory of the Contribution of Excitons to the Complex Dielectric Constant of Crystals*, Phys. Rev. **112**, 1555 (1958).

[25] C. Kittel, *Quantum Theory of Solids* (John Wiley & Sons, New York, 1963).

[26] R. H. Dicke, *Coherence in Spontaneous Radiation Processes*, Phys. Rev. **93**, 99 (1954).

[27] S. Maier, *Plasmonic Field Enhancement and SERS in the Effective Mode Volume Picture*, Opt. Express **14**, 1957 (2006).

[28] R. Feynman, *The Feynman Lectures on Physics: Mainly Electromagnetism and Matter*, Vol. 2 (Addison-Wesley, Reading Massachusetts, 1964).

[29] S. Haroche, in *Fundamental Systems in Quantum Optics, Les Houches Session LIII*, edited by J. Dalibard, J.-H. Raimond, and J. Zinn-Justin (North-Holland, Amsterdam, 1992).

[30] J. D. Jackson, *Classical Electrodynamics* (Wiley, New York, 1998).

[31] J. M. Gérard, B. Sermage, B. Gayral, B. Legrand, E. Costard, and V. Thierry-Mieg, *Enhanced Spontaneous Emission by Quantum Boxes in a Monolithic Optical Microcavity*, Phys. Rev. Lett. **81**, 1110 (1998).

[32] M. Babiker and R. Loudon, *Derivation of the Power-Zienau-Woolley Hamiltonian in Quantum Electrodynamics by Gauge Transformation*, Proc. R. Soc. A **385**, 439 (1983).

[33] C. Cohen-Tannoudji, J. Dupont-Roc, and G. Grynberg, *Photons et Atomes* (EDP Sciences/CNRS Editions, Paris, 2001).

[34] J. Keeling, *Coulomb Interactions, Gauge Invariance, and Phase Transitions of the Dicke Model*, J. Phys. Condens. Matter **19**, 295213 (2007).

[35] Y. Todorov and C. Sirtori, *Intersubband Polaritons in the Electrical Dipole Gauge*, Phys. Rev. B **85**, 045304 (2012).

[36] W. H. Louisell, *Quantum Statistical Properties of Radiation* (John Wiley & Sons, New York, 1973).

[37] L. J. Chu, *Physical Limitations of Omnidirectional Antennas*, J. Appl. Phys. **19**, 1163 (1948).

[38] M. H. Devoret, in *Quantum Fluctuations*, edited by S. Reymaud, E. Giacobino, and J. Zinn-Justin (Elsevier, New York, 1997).

[39] M. Gross and S. Haroche, *Superradiance: An Essay on the Theory of Collective Spontaneous Emission*, Phys. Rep. **93**, 301 (1982).

[40] E. Strupiechonski, G. Xu, M. Brekenfeld, Y. Todorov, N. Isac, A. M. Andrews, P. Klang, C. Sirtori, G. Strasser, A. Degiron, and R. Colombelli, *Sub-diffraction-limit Semiconductor Resonators Operating on the Fundamental Magnetic Resonance*, Appl. Phys. Lett. **100**, 131113 (2012).

[41] S. S. Mohan, M. del Mar Hershenson, S. P. Boyd, and T. H. Lee, *Simple Accurate Expressions for Planar Spiral Inductances*, IEEE J. Solid-State Circuits **34**, 1419 (1999).

[42] W.-C. Chen, C. M. Bingham, K. M. Mak, N. W. Caira, and W. J. Padilla, *Extremely Subwavelength Planar Magnetic Metamaterials*, Phys. Rev. B **85**, 201104 (2012).

[43] D. Dietze, A. Benz, G. Strasser, K. Unterrainer, and J. Darmo, *Terahertz Meta-atoms Coupled to a Quantum Well Intersubband Transition*, Opt. Express **19**, 13700 (2011).

[44] A. Benz, S. Campione, S. Liu, I. Montano, J. F. Klem, A Allerman, J. R. Wendt, M. B. Sinclair, F. Capolino, and I. Brener, *Strong Coupling in the Sub-wavelength Limit Using Metamaterial Nanocavities*, Nat. Commun. **4**, 2882 (2013).

[45] C. Jansen, I. A. I. Al-Naib, N. Born, and M. Koch, *Terahertz Metasurfaces with High Q-factors*, Appl. Phys. Lett. **98**, 051109 (2011).

[46] M. I. Amant, A. Bismuto, M. Beck, L. Isa, K. Kumar, E. Reimhult, and J. Faist, *Electrically Driven Nanopillars for THz Quantum Cascade Lasers*, Opt. Express **21**, 10917 (2013).

[47] I. Yeo, N. S. Malik, M. Munsch, E. Dupuy, J. Bleuse, Y.-M. Niquet, J.-M. Gérard, J. Claudon, E. Wagner, S. Seidelin, A. Auffèves, J.-P. Poizat, and G. Nogues, *Surface Effects in a Semiconductor Photonic Nanowire and Spectral Stability of an Embedded Single Quantum Dot*, Appl. Phys. Lett. **99**, 233106 (2011).

[48] E. A. Zibik, T. Grange, B. A. Carpenter, N. E. Porter, R. Ferreira, G. Bastard, D. Stehr, S. Winnerl, M. Helm, H. Y. Liu, M. S. Skolnick, and L. R. Wilson, *Long Lifetimes of Quantum-Dot Intersublevel Transitions in the Terahertz Range*, Nat. Mater. **8**, 803 (2009).

[49] T. Ando, A. B. Fowler, and F. Stern, *Electronic Properties of Two-Dimensional Systems*, Rev. Mod. Phys. **54**, 437 (1982).

[50] Y. Todorov, L. Tosetto, A. Delteil, A. Vasanelli, C. Sirtori, A. M. Andrews, and G. Strasser, *Polaritonic Spectroscopy of Intersubband Transitions*, Phys. Rev. B **86**, 125314 (2012).

[51] A. A. Anappara, A. Tredicucci, G. Biasiol, and L. Sorba, *Electrical Control of Polariton Coupling in Intersubband Microcavities*, Appl. Phys. Lett. **87**, 051105 (2005).

[52] G. Günter, A. A. Anappara, J. Hees, A. Sell, G. Biasiol, L. Sorba, S. De Liberato, C. Ciuti, A. Tredicucci, A. Leitenstorfer, and R. Huber, *Sub-cycle Switch-on of Ultrastrong Light-Matter Interaction*, Nature (London) **458**, 178 (2009).

[53] P. Biagioni, J.-S. Huang, and B. Hecht, *Nanoantennas for Visible and Infrared Radiation*, Rep. Prog. Phys. **75**, 024402 (2012).

[54] C. Feuillet-Palma, Y. Todorov, A. Vasanelli, and C. Sirtori, *Strong Near Field Enhancement in THz Nano-antenna Arrays*, Sci. Rep. **3**, 1361 (2013).

[55] J. Casanova, G. Romero, I. Lizuain, J. J. García-Ripoll, and E. Solano, *Deep Strong Coupling Regime of the Jaynes-Cummings Model*, Phys. Rev. Lett. **105**, 263603 (2010).

[56] T. Volz, A. Reinhard, M. Winger, A. Badolato, K. J. Hennessy, E. L. Hu, and A. Imamoglu, *Ultrafast All-Optical Switching by Single Photons*, Nat. Photonics **6**, 607 (2012).

[57] T. Peyronel, O. Firstenberg, Q.-Y. Liang, S. Hofferberth, A. V. Gorshkov, T. Pohl, M. D. Lukin, and V. Vuletic, *Quantum Nonlinear Optics with Single Photons Enabled by Strongly Interacting Atoms*, Nature (London) **488**, 57 (2012).

[58] S. D. Liberato and C. Ciuti, *Stimulated Scattering and Lasing of Intersubband Cavity Polaritons*, Phys. Rev. Lett. **102**, 136403 (2009).

[59] M. D. Lukin, M. Fleischhauer, R. Cote, L. M. Duan, D. Jaksch, J. I. Cirac, and P. Zoller, *Dipole Blockade and Quantum Information Processing in Mesoscopic Atomic Ensembles*, Phys. Rev. Lett. **87**, 037901 (2001).

[60] D. Gottesman, A. Kitaev, and J. Preskill, *Encoding a Qubit in an Oscillator*, Phys. Rev. A **64**, 012310 (2001).

[61] S. D. Bartlett, H. de Guise, and B. C. Sanders, *Quantum Encodings in Spin Systems and Harmonic Oscillators*, Phys. Rev. A **65**, 052316 (2002).

[62] A. Delteil, A. Vasanelli, Y. Todorov, B. Paulillo, G. Biasiol, L. Sorba, and C. Sirtori, *Gate Controlled Coupling of Intersubband Plasmons*, Appl. Phys. Lett. **102**, 031102 (2013).

[63] T. Holstein and H. Primakoff, *Field Dependence of the Intrinsic Domain Magnetization of a Ferromagnet*, Phys. Rev. **58**, 1098 (1940).

[64] G. F. Mazenko, *Nonequilibrium Statistical Mechanics* (Wiley-VCH, Weinheim, 2006).